Available online at www.sciencedirect.com

ScienceDirect

Advances in Space Research 66 (2020) 2854–2864

ADVANCES IN SPACE RESEARCH (a COSPAR publication)

www.elsevier.com/locate/asr

A GNSS-based near real time automatic Earth Crust and Atmosphere Monitoring Service for Turkey

Gokhan Gurbuz [a,*], Bahadir Aktug [b], Shuanggen Jin [c,d], S. Hakan Kutoglu [a]

[a] Department of Geomatics Engineering, Zonguldak Bulent Ecevit University, Zonguldak 67100, Turkey
[b] Department of Geophysics Engineering, Ankara University, Ankara 06100, Turkey
[c] School of Remote Sensing and Geomatics Engineering, Nanjing University of Information Science and Technology, 210044, China
[d] Shanghai Astronomical Observatory, Chinese Academy of Sciences, Shanghai 200030, China

Received 21 January 2020; received in revised form 17 July 2020; accepted 18 July 2020
Available online 30 July 2020

Abstract

Turkey is located in a highly active earthquake zone. Many geodynamic and seismic activities occur during a day, such as earthquakes, landslides, sinkholes and creep movements. In addition to seismicity, Turkey has unique physical features like being surrounded by seas on three sides, affected by different climate types. It is located on mid latitudes, which makes Turkey very suitable for atmospheric studies. For this reason, Turkey serves as a natural laboratory for geodesy, geophysical and atmospheric scientists. Therefore, Global Navigation Satellite System (GNSS) data are used in many areas. However, not all the scientists can reach or process the data for coordinate-based studies. Within the scope of the study, a GNSS-based Earth Crust and Atmosphere Monitoring Service is established at the Zonguldak Bulent Ecevit University. Using the results of the GNSS processing, time series of GNSS station positions are produced and used to infer strain solutions related to earthquakes. Estimates of the Precipitable Water Vapour (PWV) and the Total Electron Content (TEC) in the ionosphere are made available for tropospheric and ionospheric studies, respectively. Visualisation of the results are intended to be provided to the scientific community. Results show that the root mean square (RMS) differences of the PWV between GNSS and radiosondes are in the range of 1–3 mm. RMS differences of the TEC is in the range of 2–3 TEC units when comparing our GNSS estimates with the Global Ionospheric Maps (GIM) from the International GNSS Service (IGS). One of the main results obtained from the analysis centre is near real-time strain rates and their relations to actual earthquakes. Results show that near real-time strain rates can be assessed as a precursor parameter for earthquakes.

Keywords: GNSS; Precipitable water vapour; Total electron content; Analysis centre

1. Introduction

According to 2018 data, 10.400 people lost their lives due to natural disasters and the global economic loss reached 160 billion dollars (URL-1). As the world population increases, the number of people affected by natural disasters increases exponentially. It is estimated that the world's population will reach 8 billion by 2030 and 10 billion by 2055 (UNDRR, 2019). Table 1 presents a statistical analysis of natural disasters and loss of life caused by natural disasters. According to this, earthquakes are one of the leading disasters in the last 20 years. This is followed by extreme temperatures, floods and storms associated with the climate. Scientists related with earth, climate and atmospheric studies are constantly researching to be prepared for disasters caused by climate change and earthquakes. In the last decades, Global Navigation Satellite System (GNSS) have become an important data source for scientists to understand geological and atmospheric phases.

* Corresponding author.
E-mail address: gokhan.gurbuz@beun.edu.tr (G. Gurbuz).

https://doi.org/10.1016/j.asr.2020.07.026
0273-1177/

Table 1
Losses caused by natural disasters between 1900 and 2018 in Turkey (Öcal, 2019).

	Event	%	Damaged Buildings	%	Demolished Buildings	%	Death	%	Injured	%
Landslide	16,223	32.7	21,334	1.6	3638	3.4	36	0,0	41	0.1
Flood	6069	12.2	62,400	4.7	507	0.5	232	0.2	116	0.2
Earthquake	3368	6.8	1,238,599	92.6	104,136	95.9	95,544	95.6	47,411	77.2
Wildfire	2256	4.6	128	0	9	0	41	0.1	42	0.1
Avalanche	1892	3.8	1179	0.1	135	0.1	128	0.1	80	0.1
Storm	1816	3.7	3648	0.3	23	0.0	264	0.3	326	0.5
Extreme Winter	845	1.7	13	0	0	0.0	143	0.1	944	1.5
Other*	17,106	34.5	10,220	0.7	125	0.1	3540	3.6	12,464	20.3
Total	49,575	100	1,337,521	100	108,573	100	99,928	100	61,424	100

* Events such as explosions, urban fires, terror related events, traffic accidents, etc.

Although it is thought that human life will not be long enough to detect and understand the Earth's crust movements that cause earthquakes, the emergence of GNSS systems has made it possible to track ground movements and understand the tectonic mechanisms much more precisely.

In the early 2000 s, conducted studies found that some earthquakes caused anomalies in the ionosphere layer before or after main shock (Liu et al., 2004; Masci and Thomas, 2015; Plotkin, 2003; Rolland et al., 2013). In addition to ionosphere, the amount of precipitable water vapour (PWV) in the troposphere layer can be determined by GNSS. It is more economical, faster, and provides much higher spatial and temporal resolution than other methods, thus making significant contributions to the forecasting of meteorological events (Baker et al., 2001; Bock and Doerflinger, 2001). In spite of these advantages provided by the GNSS for earth, climate and atmospheric scientists, the above-mentioned studies require advanced geodetic knowledge and complex academic software skills. However, it is not possible for every scientist from different disciplines to have this knowledge and skills. This situation makes it possible only for a limited number of scientists to benefit from the opportunities provided by GNSS systems and prevent its widespread usage.

As mentioned before, Turkey is located in one of the world's most troubled regions in terms of natural disasters and seismic activities. In fact, approximately 50% of the settlements in the country have been exposed to a natural disaster at least once between 1950 and 2008 (Gokce et al. 2008). It is an undisputed fact that this number has risen even higher nowadays.

In Turkey, 146 permanent GNSS stations, homogenously distributed all over the country about 80 km distance between the stations that are tracking Global Positioning System (GPS) and Globalnaya Navigatsionnaya Sputnikovaya Sistema, form CORS (Continuously Operating Reference Station) network. Moreover, the 30 s interval data of CORS-TR stations are available to scientists. This opportunity is a blessing for better understanding of natural disasters occurring in the country and for developing country policies to mitigate harm. However, in Turkey, as is in the World, the number of qualified scientists are extremely limited to process these data and obtaining the final product. The lack of an online service infrastructure that serves end users by processing the data adversely affects the natural disaster-oriented use of the GNSS infrastructure. A GNSS-based Earth Crust and Atmosphere Monitoring Service has been established, to eliminate this aforementioned lack of service infrastructure and to support all scientists from different disciplines for their research or to support the authorities in their operational activities. The system automatically computes the daily crustal movements, parametric changes in the ionosphere and the troposphere on hourly and daily basis and provides online service. In this study, the evaluation strategy and the results of this service are discussed.

2. The Turkish CORS network

The project of Turkish CORS Network (TUSAGA-Aktif in Turkish) utilised in this study was started in 2006 jointly by General Directorate of Land Registry and Cadastre (GDLRC) and General Directorate of Mapping (GDM). The system is operational to users all over the country since 2009 (Eren et al., 2009) (Fig. 1). As mentioned above, the main goal of this network is to establish network-based CORS-TR stations functioning 24/7 with RTK capabilities at centimetre accuracy level using 146 GNSS stations (Fig. 1).

The Operation of the CORS-TR system and calculation of correction parameters are performed from control centres established in GDLRC and GDM. The data collected from all stations are transferred to the data centre through ADSL (Asymmetric Digital Subscriber Line) and GPRS (General Packet Radio Service)/EDGE (Enhanced Data GSM (Global System for Mobile communication) Environment). Then, the correction parameters are calculated and transferred to the users in the field. Real-time Kinematic correction data are available in RTCM3.1 (Radio Technical Commission for Maritime) and CMR (Cellular Mobile Radio) communication formats and is sent to rover receivers through GPRS and NTRIP (Network Transport of RTCM through Internet Protocol). The corrections are sent based on VRS (Virtual Reference Stations), FKP (Flachen Korrectur Parameter), and MAC (Master Auxiliary Concept) techniques.

The geocentric datum of CORS-TR is a semi-kinematic datum implemented with respect to the International

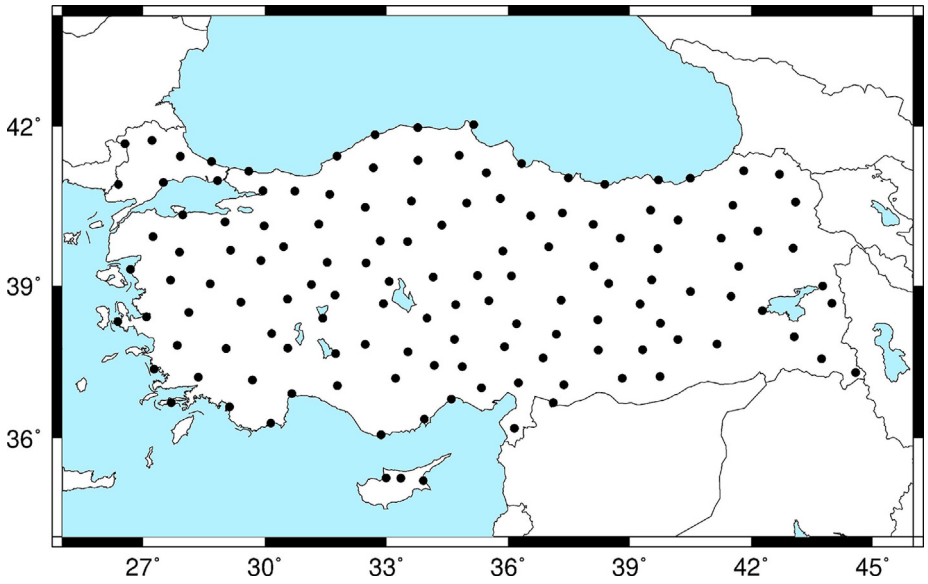

Fig. 1. CORS-TR network and its nationwide coverage.

Terrestrial Reference Frame (ITRF 96) at the reference epoch of 1 January 2005 (2005.00). ITRF No Net Rotation (NNR) velocities of CORS stations maintained this implementation. Up-to-date ITRF NNR velocities were determined by GDM in Turkey using 7 years of CORS stations data from 2008 to 2015. In accordance with Turkish surveying regulation, there are two types of coordinate computation of the control points performed with GNSS relative positioning technique based on the datum. Coordinates of the first-order and the second-order control points are computed in semi-kinematic datum, whereas the third-order control points are computed in static datum. Generally, GNSS stations are used as fiducial stations for coordinate computation of these control points.

3. Data and methodology

The analyses involved five main sequential phases such as, data acquisition, processing, atmospheric parameter estimation, visualizing the results and transmitting the results to the end user on the web (Fig. 2). In the data acquisition phase, using file transfer protocol websites, hourly GNSS data belong to IGS and CORS-TR networks, and ultra-rapid ephemeris products from IGS are downloaded.

TEQC software is being used for quality check for downloaded data. After the data are checked, the GNSS data processing procedure starts. In the processing phase, subnetworks are created with overlapping GNSS stations with same reference IGS stations. The system uses GAMIT/GlobK package software for GNSS data processing, which is used in many academic studies related to GNSS (Herring et al., 2015). Also the system uses Bernese GNSS software for ionospheric parameter estimation (Dach et al., 2007).

The important parameter for the evaluation of data for near real-time evaluations is time for processing, which is directly related with the number of sub-network and the number of GNSS stations used in the active evaluation. As the solution needs to be computed quickly in near real-time solutions, the required number of subnets has been established and these evaluations are initiated to provide the robust and fastest solution of GAMIT/GlobK.

The displacement components are computed in the ITRF2014 fixed system. The parameters, which are used in processing, are given in Table 2. Velocity vectors and PWV values obtained from the processing of each station is visualised using the GMT software (Wessel et al., 2013). Also for each station, time series are updated hourly for further analysis.

3.1. ZTD and PWV estimation

In the troposphere, PWV can be estimated using Zenith Wet Delay (ZWD). Zenith Total Delay (ZTD), can be computed directly from the GNSS signal propagation on troposphere. But wet delay is unpredictable and cannot be computed directly. That is why ZWD is estimated by subtracting hydrostatic part of the delay, which can be computed directly or taken from models, from the total delay. Unfortunately, GNSS stations used in this study are not equipped with meteorological sensors. Therefore, GPT2 model is used to compute hydrostatic delay. Using ZWD, the hourly PWV values were computed with GAMIT/GlobK (Herring et al., 2015). The relation between PWV and ZWD is expressed as Eq. (1) (Askne and Nordius, 1987; Bevis et al. 1992, 1994; Jin et al., 2009),

$$\mathrm{PWV} = \Pi \times \mathrm{ZWD} \tag{1}$$

where Π is a water vapour conversion factor, which can be expressed as Eq. (2),

$$\Pi = \frac{10^6}{\rho R^v[(k_3/T_m + k_2')]} \tag{2}$$

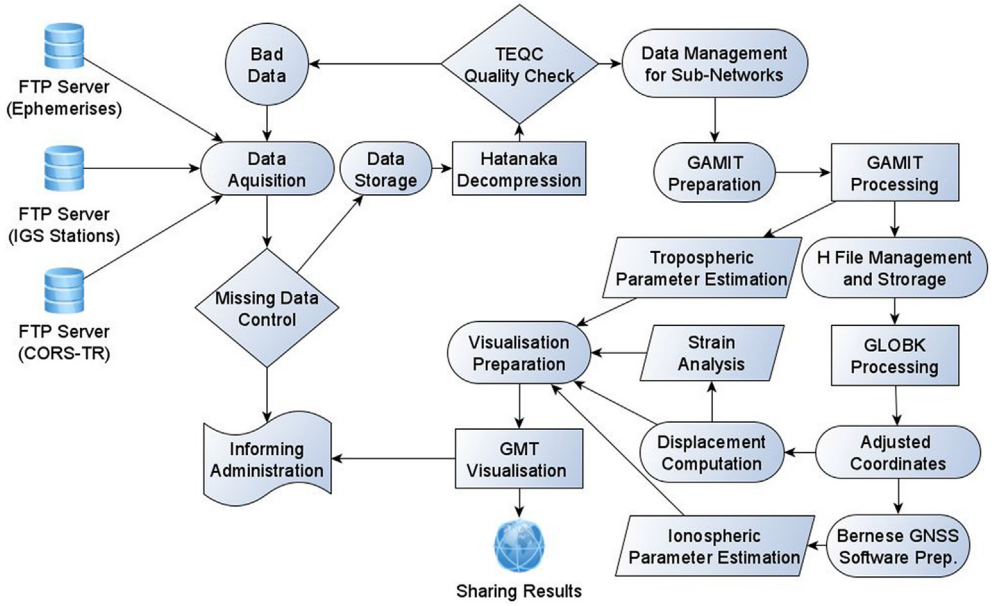

Fig. 2. Processing workflow chart of the analysis centre.

Table 2
GNSS Data processing parameters for GAMIT/GlobK.

Parameters	Used Values
Data Sampling Frequency	30 s
Cut-off of the Elevation Angle	10°
Earth Orientation Parameters	IERS Bulletin-B
Ionospheric Solution	Iono-free
High-order Ionospheric Delay	Neglected
Satellite Ephemeris	IGS Ultra Rapid
Antenna Phase Centre Model	IGS14.ATX
Tropospheric Model	GPT2
Mapping Function (Wet-Dry)	GMF
Ocean Tidal Loading	FES2004
Solar Radiation Pressure	Berne
Polar and Earth Tides	IERS03

where ρ is the density of liquid water, R_v is the specific gas constant for water vapour, k_3, k_2' are physical constants, T_m is the mean temperature of the atmosphere as Eq. (3),

$$T_m = \frac{\int (e/T)dh}{\int (e/T^2)dh} \tag{3}$$

which can be computed from surface temperature (Bevis et al., 1994). In this study, $T_m = 48.55 + 0.80 \times T_s$, which is derived from meteorological observations in Turkey (Mekik and Deniz, 2017), is used to compute PWV values.

3.2. Strain rate computation

The strains computed from displacements by the hourly, daily and cumulative GNSS data solutions provide useful information for crustal deformation studies. Strain tensors are calculated from the three-dimensional GNSS displacements using the MATLAB software (Kutoglu et al., 2016). In strain tensor computation, easy and fast Delaunay triangulation technique is used. Strains for each triangle centre points are computed hourly and daily. Therefore, continuous strains are obtained to map shear and normal strains without delving into complicated deformation computations (Hackl et al., 2009; Kutoglu et al., 2016).

The computational function uses the linear least square approach to estimate velocity gradient tensor (Pesci and Teza, 2007). After the iterations, strain computations visualised for all grid points (Pesci and Teza, 2007). Using linear interpolation for velocity components for all the axes establishes a continuous strain field under the assumption of the velocities that are independent from each other. The elasticity theory of continuum mechanics states that the displacement equation for a point i in a homogeneous deformable body is as Eq. (4),

$$u_i = c_0 + Er_i = c_0 + (S + A)r_i \tag{4}$$

where $u_i = \left[\left(x_i^2 - x_i^1\right)\left(y_i^2 - y_i^1\right)\left(z_i^2 - z_i^1\right)\right]^t$ is the displacement vector of the point i where superscripts 1 and 2 represent the first and second observation periods,c_0 is the arbitrary shift vector, S is the strain matrix and $r_i = [x_i y_i z_i]^t$ is the position vector on t epoch. Obtaining a derivative along each is possible using interpolation for the components of a velocity field (Hackl et al., 2009). Continuous velocity fields produced from all the axes represents the strain tensor by linear combination. Strain tensor parameters defined as S matrix is given in the Eq. (5),

$$S = \begin{bmatrix} \frac{\partial u_i}{\partial x} & \frac{1}{2}\left(\frac{\partial u_i}{\partial y} + \frac{\partial v_i}{\partial x}\right) & \frac{1}{2}\left(\frac{\partial u_i}{\partial z} + \frac{\partial w_i}{\partial x}\right) \\ \frac{1}{2}\left(\frac{\partial v_i}{\partial x} + \frac{\partial u_i}{\partial y}\right) & \frac{\partial v_i}{\partial y} & \frac{1}{2}\left(\frac{\partial v_i}{\partial z} + \frac{\partial w_i}{\partial y}\right) \\ \frac{1}{2}\left(\frac{\partial w_i}{\partial x} + \frac{\partial u_i}{\partial z}\right) & \frac{1}{2}\left(\frac{\partial w_i}{\partial y} + \frac{\partial v_i}{\partial z}\right) & \frac{\partial w_i}{\partial z} \end{bmatrix} \tag{5}$$

where x, y and z coordinates of the GNSS stations and $\varepsilon_{xx}\frac{\partial u_i}{\partial x}$, $\varepsilon_{yy}\frac{\partial v_i}{\partial y}$ and $\varepsilon_{zz}\frac{\partial w_i}{\partial z}$ are the normal strains associated with the x, y and z axes, $\varepsilon_{xy}=\frac{1}{2}\left(\frac{\partial u_i}{\partial y}+\frac{\partial v_i}{\partial x}\right)$, $\varepsilon_{xz}=\frac{1}{2}\left(\frac{\partial u_i}{\partial z}+\frac{\partial w_i}{\partial x}\right)$ and $\varepsilon_{yz}=\frac{1}{2}\left(\frac{\partial w_i}{\partial y}+\frac{\partial v_i}{\partial z}\right)$ are the shear strains on the planes defined by the related pair of axes. The matrix A represents the rigid body rotation. In a similar way, as shown above, it is possible to compute the antisymmetric rotation tensor given in the Eq. (6),

$$A=\begin{bmatrix} 0 & \frac{1}{2}\left(\frac{\partial u_i}{\partial y}-\frac{\partial v_i}{\partial x}\right) & \frac{1}{2}\left(\frac{\partial u_i}{\partial z}-\frac{\partial w_i}{\partial x}\right) \\ \frac{1}{2}\left(\frac{\partial v_i}{\partial x}-\frac{\partial u_i}{\partial y}\right) & 0 & \frac{1}{2}\left(\frac{\partial v_i}{\partial z}-\frac{\partial w_i}{\partial y}\right) \\ \frac{1}{2}\left(\frac{dw_i}{\partial x}-\frac{du_i}{\partial z}\right) & \frac{1}{2}\left(\frac{\partial w_i}{\partial y}-\frac{\partial v_i}{\partial z}\right) & 0 \end{bmatrix} \quad (6)$$

The Eigen space analysis of the tensor defines deformation at every grid point, providing different aspects of the strain state like maximum and minimum strains. Linear combination of the minimum and maximum Eigen values gives the maximum shear strain for every grid point, which is a way to identify active faults (Hackl et al., 2009). Strain tensors for each Delaunay triangle is computed using the coordinates and displacement vectors of the corners of triangle, which are obtained from GNSS data processing.

Projection and Cartesian coordinates of GNSS stations are calculated as a result of evaluations made with the analysis centre. For the strain parameters to be calculated daily and/or cumulatively, triangles are formed in the whole network using Delaunay Triangulation. 3-dimensional strain calculation is made based on the centres of the Delaunay Triangles created for the calculated daily and cumulative Cartesian coordinate differences. For this calculation, geocentric Cartesian coordinates are converted into topocentric coordinates. As a result, normal strains in three axes, shear stresses in the planes formed by these axes, spatial changes and changes in total volume are obtained. Fig. 3 shows the TUSAGA-Active network plotted as a result of triangulation.

After the computation of the triangles, the result files are adjusted to the GMT format to generate the interpolated strain maps using the GMT software. For normal strains on the axes: X axis (daily and cumulative), Y axis (daily and cumulative) and Z-axis (daily and cumulative) visualisations; for shear stresses in planes: XY plane (daily and cumulative), XZ plane (daily and cumulative) and YZ plane (daily and cumulative) visualisations are performed.

3.3. TEC estimation

The GNSS technique presents an opportunity for space weather monitoring by computing TEC values in near real time. TEC is calculated along the path from the receiver to the satellite in a column with a cross-sectional area of a square meter and is expressed as TECU 10^{16} electrons/m^2 (Chakraborty et al., 2014; Otsuka et al., 2002). The precision of the ionospheric TEC estimation and GNSS station distribution of the related study area directly affects the ionospheric maps, which can be produced both regionally and globally. Aside from GNSS station distribution and processing, magnetic storms, space weather-related issues, sun spots and even space shuttle launch are affecting ionospheric TEC values. Therefore, the ionosphere should be modelled correctly with respect to all the external parameters. Also modelling ionosphere precisely helps single frequency GNSS for civilian users (Allain and Mitchell, 2009, Shi et al., 2012, Zhou et al., 2020). The ionosphere introduces a frequency-dependent delay of the signal while propagating from the GNSS satellite to the receiver. Using dual frequency receivers TEC can be computed using code and phase measurements. However, both measurements have their own limitations, for example, low accuracy of the code measurement and the integer phase ambiguity of the phase measurement. Using smoothed code measurements which uses both code and phase measurements to calibrate the TEC, integer phase ambiguity problem is resolved and the accuracy reaches a sufficient level to obtain TEC variations (Cesaroni et al., 2015). Pseudorange equations from code observations given by Eqs. (7) and (8),

$$P^h_{1,a}=P^h_a+c\left(\Delta t^h-\Delta t_a\right)+I^h_{1,a}+T^h_a+d^h_1+d_{1,a}+\varepsilon^h_{P,1,a} \quad (7)$$

$$P^h_{2,a}=P^h_a+c\left(\Delta t^h-\Delta t_a\right)+I^h_{2,a}+T^h_a+d^h_2+d_{2,a}+\varepsilon^h_{P,2,a} \quad (8)$$

where P^h_a is the distance between a receiver and a satellite, c is the velocity of light, Δt^h is satellite clock error, Δt_a is receiver clock error, $I^h_{1,a}$ and $I^h_{2,a}$ ionospheric effects for their respected signal frequencies, T^h_a is tropospheric effect, d^h_1 and d^h_2 is the code delay for satellite instrument bias, $\varepsilon^h_{P,1,a}$ and $\varepsilon^h_{P,2,a}$ are biases. As for carrier phase measurements given by Eqs. (9) and (10),

$$\varphi^h_{1,a}(t)=\varphi^h_a+c\left(\Delta t^h-\Delta t_a\right)-I^h_{1,a}+T^h_a-\lambda\left(b^h_{1,a}-N^h_{1,a}\right)+\varepsilon^h_{P,1,a} \quad (9)$$

$$\varphi^h_{2,a}(t)=\varphi^h_a+c\left(\Delta t^h-\Delta t_a\right)-I^h_{2,a}+T^h_a-\lambda\left(b^h_{2,a}-N^h_{2,a}\right)+\varepsilon^h_{P,2,a} \quad (10)$$

where φ^h_a is the distance between a receiver and a satellite, $b^h_{1,a}$ and $b^h_{2,a}$ are the phase advances for satellite instrument biases, $N^h_{1,a}$ and $N^h_{2,a}$ integer phase ambiguities and λ represents the wavelength of frequency. For each satellite, slant ionospheric delay is computed and with the use of mapping function slant delays are converted to vertical delay, which represents vertical total electron content (VTEC) along the ray path. Slant total electron content (STEC) values at the analysis centre are computed by Bernese GNSS software (Dach et al., 2007). Software uses GNSS frequencies (f_1 and f_2), differences in smoothed code measurements ($P^h_{4,a}=P^h_{1,smt,a}-p^h_{2,smt,a}$), light velocity (c) and differential

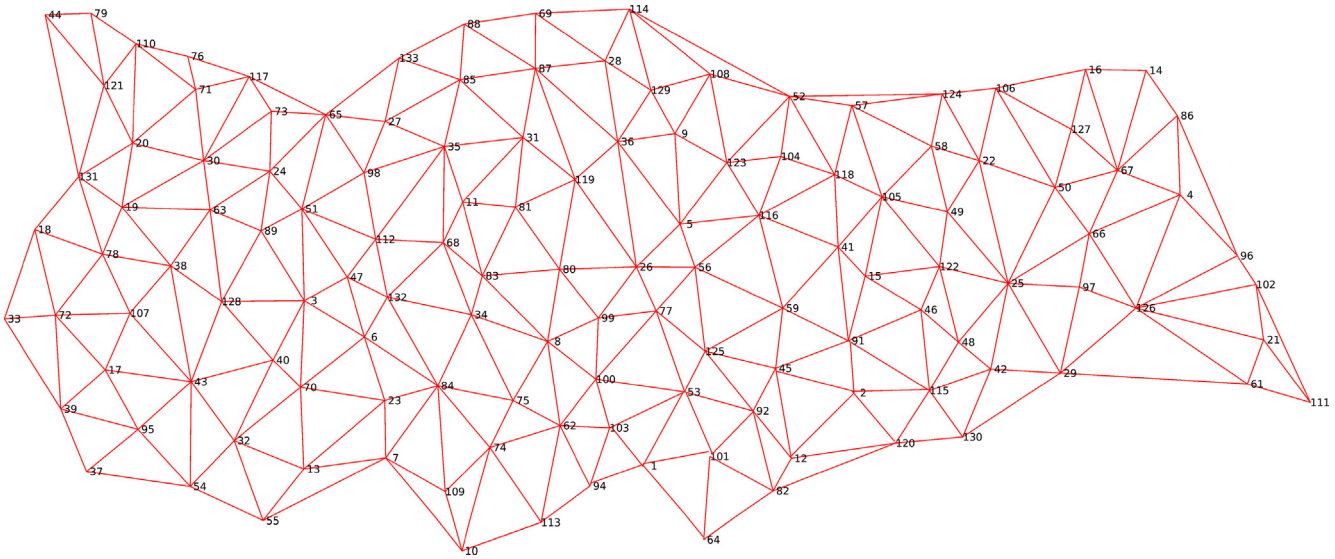

Fig. 3. Delaunay triangles of the CORS-TR network.

code bias (DCB) values are used for both the receiver and each satellite to obtain STEC values using Eq. (11). The satellite DCB values are taken from the rapid Ionosphere Map Exchange Format (IONEX) files distributed by the Center for Orbit Determination in Europe (CODE) available with one-day latency. As stated in the study of Bergeot et al, (2014), day-to-day satellite DCB variations are assumed negligible. Using the rapid IONEX product as a priori ionospheric model, the VTEC values of the Ionospheric Pierce Point (IPP) for a given receiver-satellite pair are extracted using ionospheric single thin layer hypothesis (Wild, 1994; Bergeot et al. 2011, 2014). Using VTEC values in Eq. (12), the STEC values are obtained, then the STEC values are used in Eq. (11) to obtain receiver DCB values.

$$STEC_a^h = -\frac{f_1^2 f_2^2}{40.3\left(f_1^2 - f_2^2\right)}\left(p_{4,a}^h - cDCB_a - cDCB^h\right) \qquad (11)$$

Use of mapping function can be done with the zenith angle of the specific satellite (Z), the Earth's radius (R) and thin shell height of the ionosphere (H = 450 km) as stated in Eq. (12).

$$VTEC = STECx(\cos(\arcsin\left(\frac{RxsinZ}{R+H}\right)) \qquad (12)$$

4. Results and discussion

4.1. Near real-time coordinates variations

After each processing, hourly solutions are kept and time series of coordinate components are updated per station. At the end of the day, daily solutions are processed and time series, which include daily coordinates, are updated. With both the hourly and the daily solutions available, users can obtain different kinds of data with respect to their needs. Using hourly and daily solutions, hourly and daily displacements are computed. Using daily solutions, cumulative displacement vectors for a decided epoch are computed and visualised using the GMT software (Fig. 4). With such a visualisation, users can see both daily and cumulative displacements for both horizontal and vertical components.

In the eastern and northern regions, the displacements are higher, while in the western and southern regions of Turkey, displacements approach to zero. The amount of displacement found agrees with previous academic studies (Aktuğ et al. 2011). The velocity components shown are calculated in the ITRF fixed system. According to the faster movement of the Arabian plate with respect to African plate, displacements of Turkey's eastern regions are bigger than western regions. While the movement in the areas to the right of the Eastern Anatolian Fault line increases in the right direction, the movement in the Central Anatolia Region approaches zero and in the Aegean Region, the direction of movement changes to the west. The reason that the movements in the Black Sea Region are faster than the Aegean and Central Anatolia Regions is that the Eurasian Plate compresses the Anatolian Block.

4.2. PWV products

Related studies of GNSS-estimated PWV shows that when radiosonde PWV is used as reference data, GNSS-PWV accuracy is under 2 mm for the daily solutions (Gurbuz and Jin, 2016, 2017). Nowadays in Turkey, mostly iMS-100 radiosonde is being used to observe meteorological parameters two times in a day. Technical specifications of iMS-100 radiosonde, such as measurement ranges, resolutions and uncertainties according to the manufacturers catalogue are given in Table 3 (Kizu et al., 2018).

PWV values obtained from nine radiosonde stations in Turkey are compared with PWV values estimated from nearly colocated GNSS stations data (Fig. 5). Data from

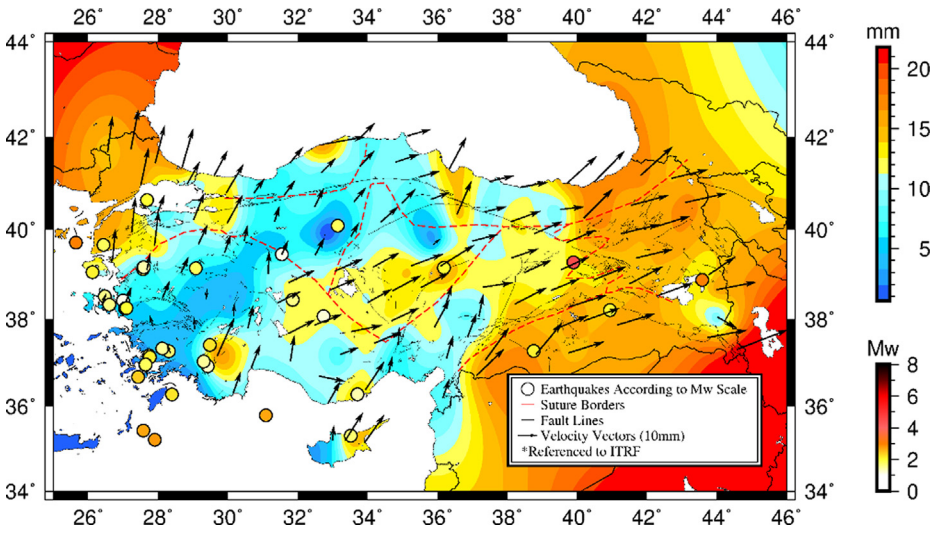

Fig. 4. Cumulative horizontal displacements for day of year 1 and 149 of 2019.

1 January 2019 to 31 September 2019 are used in the evaluations for each GNSS station. Results of the evaluations show that PWV amounts were estimated with root mean square (RMS) differences of 1.74–2.1 mm regardless of the regional climate or height differences between station locations (Table 4). This proves that even though the GNSS processing is near real-time, PWV values estimated from GNSS can be used in meteorological studies with high spatial and temporal resolutions with respect to radiosondes. However, to see the actual performance of the near real-time solution, a secondary strategy is implemented to the system, which postprocesses the data using final ephemeris and clock products (Table 4).

4.3. TEC variations

In the analysis centre, two-hourly GNSS TEC values are computed using local CORS network and linear interpolation maps are generated for users to observe ionospheric variations over the study area (Fig. 6). Additionally, earthquakes occurred a day before the generated ionospheric map also marked at the map to relate TEC values with earthquakes.

Near real-time GNSS estimated TEC values are compared with the rapid IGS GIM TEC values. The rapid IGS GIM, provided with daily, has a time resolution of 2 h and an estimated accuracy of 2–8 TECU and grid spacing 5° by 2.5° in longitude and latitude. The result shows that average differences with near real-time GNSS TEC values and rapid IGS GIM 0.4 TECU and RMS of the differences between datasets is 0.61 TECU for a randomly picked station. This proves that the analysis centre computes TEC values with sufficient accuracy with respect to the rapid IGS GIM products. The time series of the TEC values from GNSS stations are updated hourly and daily after each processing (Fig. 7).

4.4. Strain rates and risk evaluation

Turkey's physical structure, particularly the coastlines are formed by the plate movements, which are the Eurasian Plate in the north, the Arabic and African plates in the

Table 3
Technical specifications of iMS-100 radiosonde.

Parameter	Height (km)	Uncertainty	Resolution	Measurement Range
Pressure	0–10	3 hPa	0.1 hPa	1050.0–3.0 hPa
	10–16	2 hPa		
	16–24	1 hPa		
	24–32	0.4 hPa		
Temperature	0–16	1 K	0.1℃	−90.0 ℃ to +60.0 ℃
	Above 16	2 K		
Relative Humidity	0–12	15% RH	0.1% RH	0% RH–100% RH
	12–17	30% RH		
Wind Speed	0–16	2 m/s	0.01 m/s	0.00–200.00 m/s
	Above 16	4 m/s		
Wind direction	0–16	10° at <10 m/s 4° at >10 m/s	0.01°	0.01–360.00°
	Above 16	20° at <10 m/s 8° at >10 m/s		

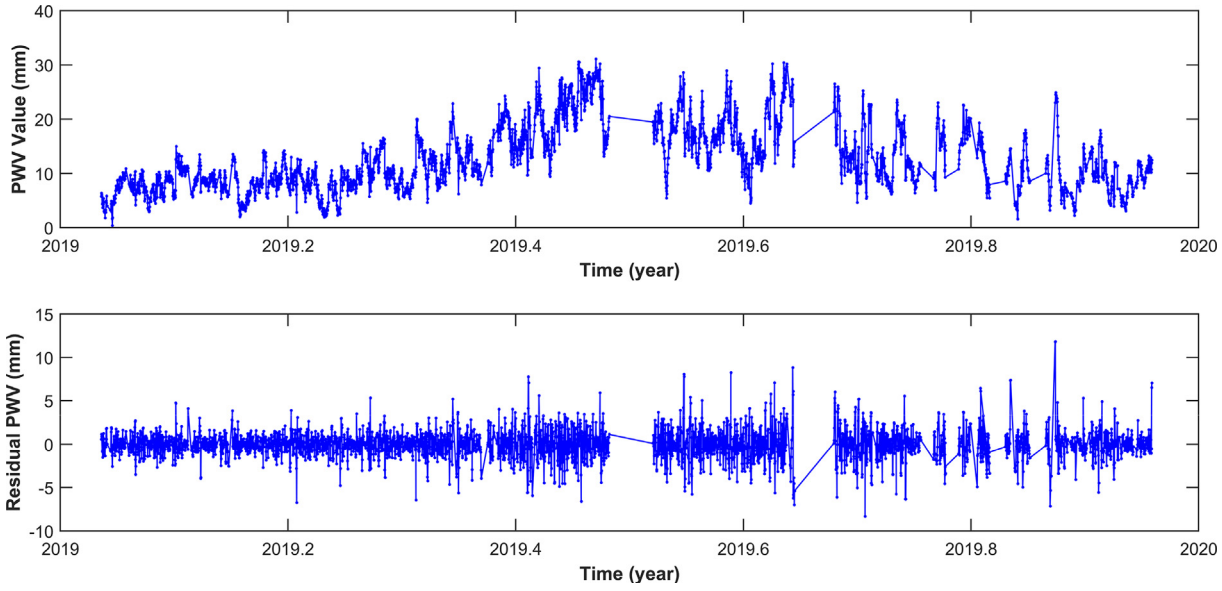

Fig. 5. Example of near real-time PWV estimation of the ANRK GNSS station.

Table 4
Comparison between GNSS estimated PWV and Radiosonde PWV values.

		NRT Processing		Post-processing	
Station	Distance (km)	Correlation	RMS (mm)	Correlation	RMS (mm)
Samsun	8.00	0.85	2.10	0.91	1.98
Istanbul	28.00	0.84	2.07	0.90	1.90
Ankara	0.10	0.84	1.74	0.90	1.64
Erzurum	0.10	0.80	1.86	0.86	1.78
Diyarbakir	5.40	0.85	1.88	0.91	1.80
Kayseri	8.00	0.75	2.10	0.87	1.99
Isparta	0.10	0.83	1.98	0.89	1.94
Izmir	0.01	0.80	1.92	0.86	1.82
Adana	13.00	0.85	1.74	0.91	1.68

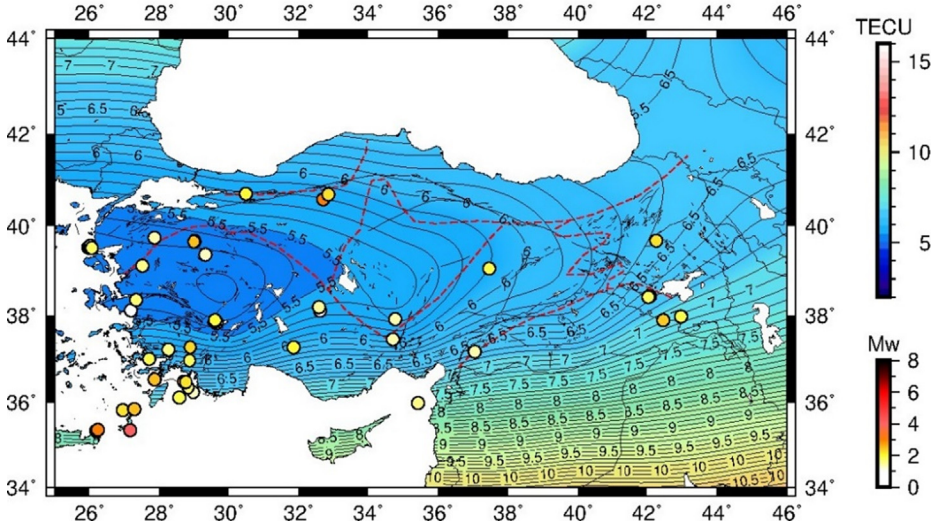

Fig. 6. Example of an ionospheric TEC map generated for 14:00 UTC of day of year 337 of 2019.

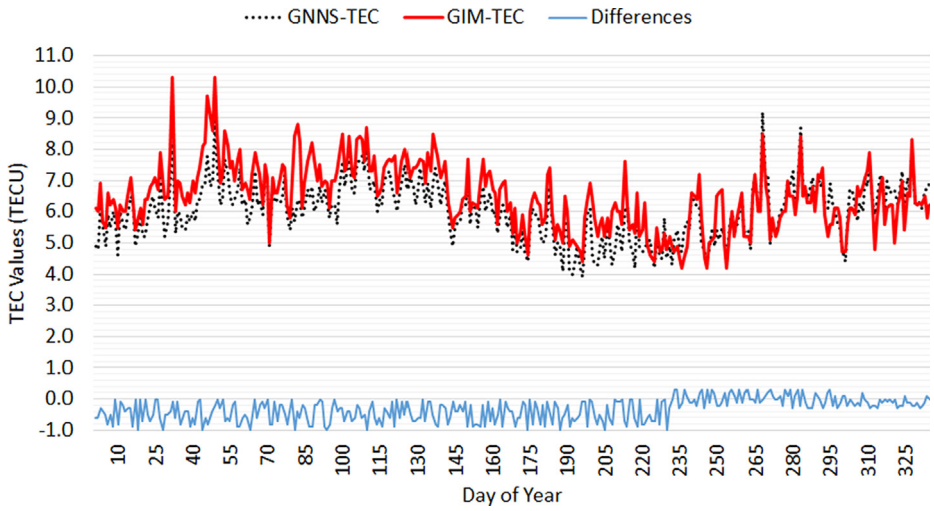

Fig. 7. TEC estimation of the ZONG GNSS station only for 14:00 UTC values for 2019.

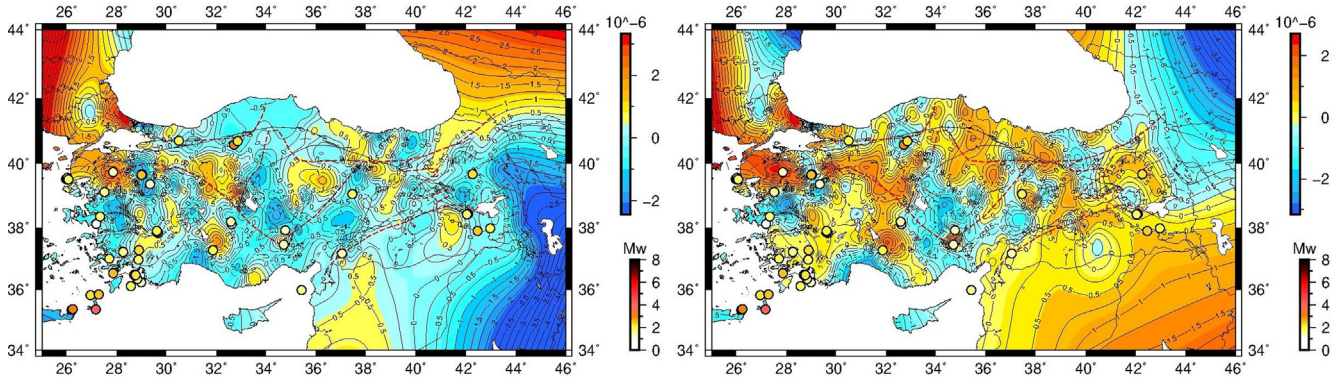

Fig. 8. Interpolation maps of cumulative normal strain for y-axis (left) and x-axis (right) for day of year 1 and 337 of 2019.

south. Additionally, the mountain structure in Turkey (east–west direction) is also associated with the movement of the plates. The expansion and compression of the Earth's crust in different axes and planes are obtained within the scope of the study that confirm this information.

The results of normal strains at Y-axis (north–south direction) show that except the northern part of the Aegean Region and western part of the Marmara Region, a large part of Turkey is covered with compression zones as in the northern part of the East Anatolian Region. While in X-axis (east–west direction), there are expansion zones near the East Anatolian Fault, the expansion and compression zones follow each other along the North Anatolian Fault (Fig. 8). In the western part of the North Anatolian Fault expansion zones it can be seen that there have been major earthquakes that have occurred in the past and that are expected to occur in the future, such as in Izmit and Yalova.

5. Conclusions and future work

Fully automatic near real-time GNSS-based Earth Crust and Atmosphere Monitoring Service is established and operational since 1 January 2019 at the Zonguldak Bulent Ecevit University. The capability of the new system is shown with different examples of products. Accuracy assessments of by-products such as PWV and TEC parameters have been done.

Apart from atmospheric parameters, cumulative strain rates for axes and planes obtained from hourly displacements also complies with the current physical structure of Turkey and the seismicity of major faults. In addition to earthquake-related studies, it is planned to carry out studies with the analysis centre in other tectonic applications, such as landslide zones or sinkhole areas where vertical displacements are important. To achieve such micro network-related studies, new stations and even new regional GNSS networks will be included in the analysis centre.

In the future, it is planned to include the seismograph data and tide gauge data in the analysis and to associate them with the existing results, to examine the characteristics of the locations where the GNSS stations are located by adding historical data to the system. The authors also recommend that related scientists should follow "http://afetmerkezi.beun.edu.tr/" website who want to examine or use daily solutions obtained by the analysis centre and

reach current or past solutions within the scope of this study.

Declaration of Competing Interest

The authors declare that they have no known competing financial interests or personal relationships that could have appeared to influence the work reported in this paper.

Acknowledgement

This study is conducted at the Zonguldak Bulent Ecevit University as a part of Ph.D. thesis titled "Automatic Processing and Analysis of Continuous GNSS Observation in Turkey." The authors are grateful to the organisations that provided the data, including the General Directorate of Mapping and General Directorate of Land Registry and Cadastre (Turkey), the International GNSS Service and the EUREF Permanent Network.

Appendix A. Supplementary material

Supplementary data to this article can be found online at https://doi.org/10.1016/j.asr.2020.07.026.

Reference

Aktuğ, B., Sezer, S., Özdemir, S., Lenk, O., ve Kılıçoğlu, A., 2011. Türkiye Ulusal Temel GPS Ağı Güncel Koordinat ve Hızlarının Hesaplanması (Computation of the Actual Coordinates and Velocities of Turkish National Fundamental GPS Network). Harita Dergisi 145, 1–14.

Allain, D.J., Mitchell, C.N., 2009. Ionospheric delay corrections for single-frequency GPS receivers over Europe using tomographic mapping. GPS Solutions 13 (2), 141–151. https://doi.org/10.1007/s10291-008-0107-y.

Askne, J., Nordius, H., 1987. Estimation of tropospheric delay for microwaves from surface weather data. Radio Sci. 22 (3), 379–386. https://doi.org/10.1029/RS022i003p00379.

Baker, H.C., Dodson, A.H., Penna, N.T., Higgins, M., Offiler, D., 2001. Ground-based GPS water vapour estimation: potential for meteorological forecasting. J. Atmos. Sol. Terr. Phys. 63 (12), 1305–1314. https://doi.org/10.1016/S1364-6826(00)00249-2.

Bergeot, N., Bruyninx, C., Defraigne, P., Pireaux, S., Legrand, J., Pottiaux, E., Baire, Q., 2011. Impact of the Halloween 2003 ionospheric storm on kinematic GPS positioning in Europe. GPS Solutions 15 (2), 171–180. https://doi.org/10.1007/s10291-010-0181-9.

Bergeot, N., Chevalier, J.M., Bruyninx, C., Pottiaux, E., Aerts, W., Baire, Q., Legrand, J., Defraigne, P., Huang, W., 2014. Near real-time ionospheric monitoring over Europe at the Royal Observatory of Belgium using GNSS data. J. Space Weather Space Clim. 2014 (4), A31. https://doi.org/10.1051/swsc/2014028.

Bevis, M., Businger, S., Herring, T.A., Rocken, C., Anthes, R.A., Ware, R.H., 1992. GPS meteorology: remote sensing of atmospheric water vapour using the global positioning system 787–15 801. J. Geophys. Res. 97(D14):15. https://doi.org/10.1029/92JD01517.

Bevis, M., Chiswell, S., Hering, T.A., Anthes, R., Rocken, C., Ware, R., 1994. GPS meteorology: mapping zenith wet delays onto precipitable water. J. Appl. Meteorol. 33, 379–386. https://doi.org/10.1175/1520-0450(1994)033<0379:GMMZWD>2.0.CO;2.

Bock, O., Doerflinger, E., 2001. Atmospheric modeling in GPS data analysis for high accuracy positioning. Phys. Chem. Earth Part A. 26 (6–8), 373–383. https://doi.org/10.1016/S1464-1895(01)00069-2.

Cesaroni, C., Spogli, L., Alfonsi, L., De Franceschi, G., Ciraolo, L., Monico, J.F.G., Bougard, B., 2015. L-band scintillations and calibrated total electron content gradients over Brazil during the last solar maximum. J. SpaceWeather Space Clim. 5 (A36), 1–11. https://doi.org/10.1051/swsc/2015038.

Chakraborty, M., Kumar, S., De, B.K., Guha, A., 2014. Latitudinal characteristics of GPS derived ionospheric TEC: a comparative study with IRI 2012 model. Ann. Geophys. 57 (5), 539. https://doi.org/10.4401/ag-6438.

Dach, R., Hugentobler, U., Fridez, P., Meindl, M., 2007. Bernese GPS Software Version 5.0. Astronomical Institute. University of Bern, Switzerland, pp. 279–286.

Mekik, C., Deniz, I., 2017. Modelling and validation of the weighted mean temperature for Turkey. Meteorol. Appl. 24 (1), 92–100. https://doi.org/10.1002/met.1608.

Eren, K., Uzel, T., Gulal, E., Yildirim, O., Cingoz, A., 2009. Results from a comprehensive Global Navigation Satellite System test in the CORS-TR network: Case study. J. Surv. Eng. 135 (1), 10–18. https://doi.org/10.1061/(ASCE)0733-9453(2009)135:1(10).

Gokce, O., Ozden, S., Demir, A., 2008. Türkiye'de Afetlerin Mekansal ve İstatiksel Dağılımı Afet Bilgileri Envanteri (Spatial and Statistical Distribution of Disasters in Turkey, Inventory of Disaster Information). Bayındırlık ve İskan Bakanlığı Afet İşleri Genel Müdürlüğü, Ankara.

Gurbuz, G., Jin, S.G., 2016. Evaluation of ocean tide loading effects on GPS-estimated precipitable water vapour in Turkey. Geod. Geodyn. 7, 32–38. https://doi.org/10.1016/j.geog.2015.12.008.

Gurbuz, G., Jin, S., 2017. Long-time variations of precipitable water vapour estimated from GPS, MODIS and radiosonde observations in Turkey. Int. J. Climatol. 37 (15), 5170–5180. https://doi.org/10.1002/joc.5153.

Hackl, M., Malservisi, R., Wdowinski, S., 2009. Strain rate patterns from dense GPS networks. Nat Hazard Earth Sys 9, 1177–1187. https://doi.org/10.5194/nhess-9-1177-2009.

Herring, T.A., King, R.W., McClusky, S.C., 2015. Introduction to GAMIT/GLOBK 10.6. Mass. Inst. of Tech., Cambridge.

Jin, S.G., Luo, O.F., Gleason, S., 2009. Characterization of diurnal cycles in ZTD from a decade of global GPS observations. J. Geod. 83, 537–545. https://doi.org/10.1007/s00190-008-0264-3.

Kizu, N., Sugidachi, T., Kobayashi, E., Hoshino, S., Shimizu, K., Maeda, R., Fujiwara, M., 2018. Technical characteristics and GRUAN data processing for the Meisei RS-11G and iMS-100 radiosondes. Gruan Technical Document, Gruan Lead Centre.

Kutoglu, H.S., Toker, M., Mekik, C., 2016. The 3-D strain patterns in Turkey using geodetic velocity fields from the RTK-CORS (TR) network. J. Afr. Earth Sc. 115, 246–270. https://doi.org/10.1016/j.jafrearsci.2015.12.002.

Liu, J.Y., Chuo, Y.J., Shan, S.J., Tsai, Y.B., Chen, Y.I., 2004. Pre-earthquake ionospheric anomalies registered by continuous GPS TEC measurements. Annales Geophysicae, European Geosciences Union 22 (5), 1585–1593.

Masci, F., Thomas, J.N., 2015. On the reliability of the Spatial Scintillation Index to detect earthquake precursors in the ionosphere. Radio Sci. 50, 745–753. https://doi.org/10.1002/2015RS005734.

Otsuka, Y., Ogawa, T., Saito, A., Tsugawa, T., Fukao, S., Miyazaki, S., 2002. A new technique for mapping of total electron content using GPS network in Japan. Earth Planets Space 54, 63–70. https://doi.org/10.1186/BF03352422.

Öcal, A., 2019. Natural Disasters in Turkey: Social and Economic Perspective. Int. J. Dis. Risk Manage. 1 (1), 51–61. https://doi.org/10.18485/ijdrm.2019.1.1.3.

Pesci, A., Teza, G., 2007. Strain rate analysis over the central Apennines from GPS velocities: the development of new free software. B Geode Sc. Aff. 56, 69–88.

Plotkin, V.V., 2003. GPS detection of ionospheric perturbation before the 13 February 2001, El Salvador earthquake. Natural Hazards and Earth System Science, Copernicus Publications on behalf of the European Geosciences Union 3(3/4), 249–253.

Rolland, L.M., Vergnolle, M., Nocquet, J.M., Sladen, A., Dessa, J.X., Tavakoli, F., Nankali, H.R., Cappa, F., 2013. Discriminating the tectonic and non-tectonic contributions in the ionospheric signature of the 2011, Mw7.1, dip-slip Van earthquake. Eastern Turke. Geophys. Res. Lett. 40, 2518–2522. https://doi.org/10.1002/grl.50544.

Shi, C., Gu, S., Lou, Y., Ge, M., 2012. An improved approach to model ionospheric delays for single-frequency precise point positioning. Adv. Space Res. 49 (12), 1698–1708. https://doi.org/10.1016/j.asr.2012.03.016.

United Nations Office for Disaster Risk Reduction, 2019. Global Assesment Report on Disaster Risk Reduction, United Nations.

URL-1 https://www.munichre.com/en/media-relations/publications/press-releases/2019/2019-01-08-press-release/index.html.

Wessel, P., Smith, W.H.F., Scharroo, R., Luis, J.F., Wobbe, F., 2013. Generic Mapping Tools: Improved version released. EOS Trans. AGU 94, 409–410. https://doi.org/10.1002/2013EO450001.

Wild, U., 1994. Ionosphere and geodetic satellite systems: permanent GPS tracking data for modelling and monitoring. Geodatischgeophysikalische Arbeiten in der Schweiz, vol. 48, Schweizerische Geodatische Kommission, Ph.D. thesis.

Zhou, P., Wang, J., Nie, Z., Gao, Y., 2020. Estimation and representation of regional atmospheric corrections for augmenting real-time single-frequency PPP. GPS Solu. 24 (1), 7. https://doi.org/10.1007/s10291-019-0920-5.